Journal of Energy Storage 152 (2026) 120430

Contents lists available at ScienceDirect

Journal of Energy Storage

journal homepage: www.elsevier.com/locate/est

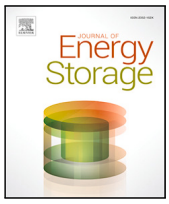

Research papers

Historical data-driven self-learning control of battery charging with convex mapping constraints

Xiaofei Han [a], Kang Li [a,*], Furong Gao [b,*], Yuanqiang Zhou [c]

[a] School of Electronic and Electrical Engineering, University of Leeds, Leeds, LS2 9JT, United Kingdom
[b] Department of Chemical and Biological Engineering, Hong Kong University of Science and Technology, Hong Kong
[c] College of Electronic and Information Engineering, Tongji University, Shanghai, 201804, China

ARTICLE INFO

Keywords:
Data-driven control
Self-learning control
Lithium-ion battery
Battery charging process
Battery management system

ABSTRACT

Thermal conditions significantly influence the battery performance and degradation, and thermal management is vital for the safe, efficient, and reliable operation of battery-powered systems such as grid-tied energy storage and electric vehicles. However, it is challenging to achieve rapid charging while minimizing the thermal impact on battery health, particularly the more critical internal battery temperature is often overlooked. Therefore, an intelligent charging control strategy is essential for effectively managing the thermal effects and enhancing charging efficiency. Given that battery charging is a highly repetitive process throughout the entire life of battery-powered systems, the historical operation data has a significant potential in the design of an effective charging control strategy. This paper proposes a novel historical data-driven self-learning control approach to iteratively optimize the battery charging strategy by applying convex mapping constraints derived from historical state information. This approach introduces a historical state convex mapping constraint, combined with a memory function to quantify the potential contribution of historical system state information and input data to improve the future control performance. The formulated historical data-based constraints and the memory function-enhanced cost function are then integrated into a model predictive control framework to optimize the battery charging current trajectories iteratively. Furthermore, to ensure that the constraints imposed on the battery electrical and thermal states are compatible with the self-learning control framework, a cascading linearized thermoelectric battery model is introduced to characterize the battery dynamics. Particularly, the internal temperature of the battery, which is not directly measurable in practical applications. Extensive simulation studies have been conducted, and the results demonstrate that the proposed control strategy can effectively regulate the internal temperature within a safe range while continuously optimizing the charging efficiency. In addition, the computation time variability is significantly reduced, with the standard deviation being decreased by approximately 80% compared to the standard MPC. The desirable control performance and continuous optimization capability make the proposed control strategy highly applicable to repetitive and complex engineering control problems.

1. Introduction

The rapid development of the lithium-ion battery technology in the past decade has made it a highly approachable solution applied in a wide range of sectors, with the aim to mitigate the environmental and air pollution issues arising from the fossil fuel-based economy [1,2]. Lithium-ion batteries are now extensively utilized in energy storage systems (ESS) [3], smart grids [4], and electric vehicles (EVs) [5]. In these applications, the battery management system (BMS) is essential to monitor battery states and manage battery operations [6]. This is particularly true for battery thermal management, which is critical in determining the performance and lifespan of batteries [7]. Excessive operations in high temperature conditions may lead to the rapid growth of the solid electrolyte interface layer and increase internal resistance, thereby reducing energy conversion efficiency. In extreme cases, high temperatures may induce the separator to melt, leading to internal short circuits and fires [8]. To mitigate these risks and ensure optimal battery performance, it is generally desirable to maintain the operating temperature within the range of 25–40 °C [9]. Achieving efficient operation with secure control strategies for lithium-ion batteries is a primary requirement for a high-performance battery management system.

* Corresponding authors.
E-mail addresses: K.Li1@leeds.ac.uk (K. Li), kefgao@ust.hk (F. Gao).

https://doi.org/10.1016/j.est.2026.120430
Received 18 September 2025; Received in revised form 21 December 2025; Accepted 5 January 2026
Available online 21 January 2026

Nomenclature

Abbreviations

BMS	Battery Management System
CC-CV	Constant Current-Constant Voltage
DASC	DAgger-Based Stochastic Control
DDC	Data-Driven Control
ESS	Energy Storage System
EVs	Electric Vehicles
FLC	Fuzzy Logic Control
GPC	General Predictive Control
ILC	Iterative Learning Control
LSTM	Long Short Term Memory
ML	Machine Learning
MPC	Model Predictive Control
P2D	Pseudo-two-Dimension
RL	Reinforcement Learning
RNN	Recurrent Neural Network
SMPC	Stochastic Model Predictive Control
SOC	State of Charge
SOH	State of Health
SPM	Single Particle Model

Symbols

$\mathbf{u}_k^*(t)$	solved optimal control input sequence (–)
Δt	sampling time interval (s)
$\mathbf{M}$	memory function set (–)
$\mathbf{X}$	historical model states set (–)
C_1	capacitance in the RC sub-circuit (F)
C_n	nominal capacity (As)
C_{p1}	heat capacity of the battery internal ($Jkg^{-1}K^{-1}$)
C_{p2}	heat capacity of the battery surface ($Jkg^{-1}K^{-1}$)
d	the window size of the historical data to be employed (–)
$diag$	diagonal matrix (–)
$i(t)$	charging current (A)
K	iteration number (–)
k_1	heat transfer coefficient between the battery internal and surface ($Wm^{-1}K^{-1}$)
k_2	heat transfer coefficient between the battery surface and ambient environment ($Wm^{-1}K^{-1}$)
N	control length (–)
N_p	prediction horizon by MPC (–)
Q, H	weighting factors in the cost function (–)
Q_J	internal resistance ohmic heat (J)
R_0	internal resistance (Ω)
R_1	resistance in the RC sub-circuit (Ω)
t	time step (–)
T_a	ambient temperature (°C)
T_{in}	battery internal temperature (°C)
T_{sf}	battery surface temperature (°C)
$u'(t)$	battery electric sub-model input (–)
$u(t)$	battery thermal sub-model input (–)
U_{ocv}	open circuit voltage (V)
V	terminal voltage (V)
V_1	voltage of the RC sub-circuit (V)

In recent decades, a wide range of approaches have been proposed to monitor and estimate the battery states, including SOC, voltage, and temperature, based on which, charging and discharging control strategies are designed. For instance, Xu et al. [10] utilized a coupled electrochemical-thermal-capacity model to optimize the charging strategy and limit the temperature rise. Liang et al. [11] developed a multilayer electrochemical-thermal coupled model for a serially connected battery module, revealing the impact of C-rate shifts during two-stage fast charging on local current density and temperature distribution, emphasizing the significance of both electrochemical performance and thermal management while designing the charging strategy. Although these models yield accurate descriptions of the battery dynamics, the complex modeling processes and significant computational demands make them impractical for real-time control applications [12]. Recent advancements in artificial intelligence have enabled the adoption of various neural networks, such as Recurrent Neural Networks (RNN) and Long Short-Term Memory (LSTM), for developing 'Black-box' battery models. Zhu et al. [13] employed data-driven methods to analyze battery thermal effects and demonstrated that an LSTM-based model accurately predicts both short-term and long-term temperature variations. Wang et al. [14] compared the back propagation neural network (BP-NN), radial basis function neural network (RBF-NN), and Elman neural network (Elman-NN) in lithium-ion battery temperature prediction within a metal foam thermal management system. Although neural network (NN)-based models have shown significant progress, their reliability still requires further validation. Furthermore, accurately capturing battery internal temperature dynamics is crucial in designing an effective charging control strategy, as the internal temperature typically rises more rapidly than the surface temperature, posing a greater risk to safety and performance. Another challenge in battery modeling is the strong coupling between electrical and thermal dynamics. The electrical model governs the voltage response to the charging current, while the thermal model describes the heat generation and dissipation, which in turn affect the battery performance and safety. The nonlinear nature of the thermal model complicates the direct integration of thermal dynamics into an efficient control framework.

Battery charging control is a critical functionality in BMS. Inappropriate charging current trajectories can significantly impact the battery performance and even accelerate battery aging. Although charging batteries with a high current could achieve a fast charging speed, it also significantly raises the battery temperature, particularly the internal temperature. If the battery temperature exceeds its operational range, the battery state of health (SOH) may suffer considerable deterioration [15]. This is however challenging to achieve a rapid charging while imposing the minimal thermal impact on the battery health. Numerous control approaches have been studied to optimize the battery charging process. For instance, Zou et al. [16] developed a model predictive control (MPC) framework applied to a simplified battery model, taking into account the mutual impact of SOC and SOH during the charging process. Tian et al. [17] introduced a battery charging methodology based on an explicit MPC, which employs piecewise linearization of the original nonlinear battery model to curtail computational expenses. The fuzzy logic control (FLC) is also widely adopted in BMS due to its high performance in managing complex nonlinear systems. Hsieh et al. [18] conducted a thorough investigation into the deployment of FLC within BMS, proposing a FLC-based charging controller for lithium-ion batteries designed to regulate the charging activities securely within a safe operational range. Rahim et al. [19] employed a boost-buck converter and developed a real-time fuzzy logic controller based on battery states, which achieves precise modulation of the pulse width

modulation (PWM) duty cycle. However, most control strategies focus on algorithm architecture and control logic, often overlooking the large amounts of historical data accumulated during each charging cycle, which can have significant potential for continuously optimizing the charging current trajectory. Although some data-driven methodologies have been explored for BMS, their applications are mainly limited to battery modeling for accurate battery state estimation [20–22]. A notable research gap remains in utilizing historical data to refine the control algorithm design, which could substantially enhance the control performance and robustness of the controller.

Most battery charging control strategies rely on analytical methods [23], while the integration of data-driven techniques for optimizing charging currents with respect to internal temperature management remains unexplored. Data-driven control (DDC) algorithms extract latent system characteristics from historical data to enhance the control adaptability and performance. One of the DDC approaches is integrating the historical information into the model construction in the control framework. For instance, Rueda-Escobedo et al. [24] formulated a DDC algorithm for discrete time-delay systems, which integrates historical data information into the model development and the state feedback gain design. In some direct DDC methodologies, the configuration and parameters of the control framework are ascertained directly from the empirical system data [25]. Persis et al. [26] employed the input and output data to formulate a data-dependent system matrix, avoiding the intricate process of physical modeling and parameter identification. However, these data-driven algorithms remain primarily focused on system dynamic modeling and parameter identification, with limited contributions to the development of the control structure and logic.

In recent years, reinforcement learning-based (RL-based) control approaches have been widely adopted to learn optimal control strategies by evaluating the action cost through the value function. However, the reinforcement learning strategy is hampered by low learning efficiency and high computational demands. The iterative learning control (ILC) progressively approaches the optimal control performance by continuously correcting control inputs using historical error information, but it does not support real-time prediction and optimization of the system behavior. The model predictive control (MPC) has emerged as a widely adopted control algorithm in practical engineering systems, attributing to its excellent flexibility in dealing with input and state constraints [27]. For instance, Drgoňa et al. [28] conducted an extensive study on the deployment of MPC in building energy control, covering a range of topics including modeling, simulation, and the design of control algorithms, providing a valuable framework for the application of MPC in relevant domains. Karamanakos et al. [29] explored the implementation of both direct and indirect MPC within the realm of power electronics control, and a comprehensive analysis of the stability and computational complexity of the MPC was conducted. However, a significant limitation of MPC is its strong reliance on the accuracy of the underlying model. The fusion of the latest data-driven technology with the MPC framework to solve complex control problems is becoming an emerging hot field of research [30].

To address the aforementioned challenges, a historical data-driven self-learning control strategy is proposed for the battery charging process. By incorporating a memory function that evaluates the contribution of past actions and iteratively refines the search space, the proposed method avoids the blind exploration typical of RL approaches and significantly reduces the computational burden. Furthermore, the integration of iterative optimization within the model predictive control framework enables the control strategy to achieve superior predictive performance and enhanced robustness for engineering systems featuring parameter uncertainty and various operating conditions.

The primary objective of this work is to charge the battery SOC from an initial state to a desired target while limiting the rise in battery cell internal temperature. In addition, charging speed is incorporated as a key element of the overall control objective. Motivated by the basic principles of ILC and MPC, a historical data-driven self-learning control strategy is proposed for the battery charging management. The proposed method introduces a novel historical-state convex mapping constraint together with a memory function embedded in the cost function. This memory function quantitatively captures the contribution of historical state and input information, enabling the controller to progressively refine the input trajectory. Furthermore, to guarantee compatibility with the constraint-handling mechanisms, a cascaded linearized thermo-electric battery model is formulated. This model ensures that constraints on both the electrical and thermal states, particularly internal temperature and terminal voltage, are accurately enforced throughout the charging process. By leveraging historical state information, the proposed framework iteratively optimizes the control input trajectory, achieving precise and efficient charging regulation. Finally, comprehensive studies are performed to evaluate the control performance and computational efficiency of the proposed approach. The results demonstrate that the method can effectively optimize control inputs without incurring additional computational burden relative to a standard MPC.

The remainder of this paper is organized as follows: Section 2 presents the cascading linearized thermoelectric battery model. Section 3 illustrates the development of the historical state convex mapping constraints and the formulation of the memory function. Section 4 illustrates the overall framework of the proposed historical data-driven self-learning control for the battery charging process. Section 5 discusses the results and analysis. Finally, Section 6 concludes this paper.

2. Cascading linearized thermoelectric battery model

The battery charging process is inherently complex, involving coupled interactions among several key variables, including the SOC, terminal voltage, and internal temperature. A major challenge in developing model-based battery charging control strategies lies in the strong coupling between the electrical and thermal dynamics. Furthermore, the nonlinear nature of battery thermal dynamics makes it challenging to incorporate the associated constraints directly into a standard linear MPC framework. To address this issue, a cascading linearized thermoelectric battery model is developed to decouple the electrical and thermal sub-models. Specifically, the thermal dynamics are reformulated as a linear model with respect to the squared charging current. The resulting linearized thermal model is then cascaded with the electrical model. By embedding this cascaded model into the proposed self-learning MPC framework, the approach enables more efficient constraint handling and improves the coordination between both the thermal and electrical objectives.

2.1. Battery electric circuit model

Generally speaking, the models for $LiFePO_4$ battery cells can be categorized into electrochemical models, equivalent circuit models, and data-driven neural models. Electrochemical models are more accurate in capturing the battery states, but are computationally expensive, making them not suitable for real-time control applications [31]. The neural network-based models are regarded as 'Black-Box' approaches, limiting their reliability and interpretability within the control framework. In contrast, the equivalent circuit model has been widely adopted due to the simple structure and straightforward parameter identification, while retaining a comparable accuracy [32]. A first-order equivalent circuit model (Thevenin circuit model) is illustrated in Fig. 1, U_{ocv} denotes the open-circuit voltage of the battery, which corresponds to the terminal voltage when the battery does not have any external load. V and i represent the terminal voltage and current, respectively. R_0 is the internal resistance of the battery. The RC sub-circuit is used to characterize the battery relaxation effect. Based on this circuit model,

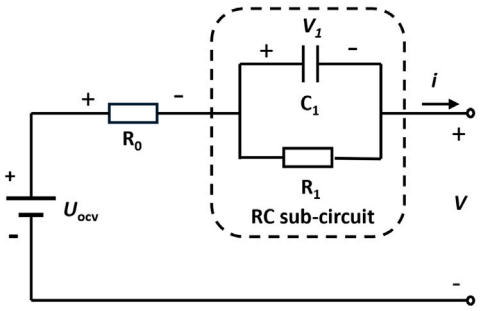

Fig. 1. Thevenin circuit model.

the corresponding discrete-time formulations can be derived as follows:

$$\begin{aligned} soc(t) &= soc(t-1) - \Delta t/C_n * i(t-1) \\ &= soc(t_0) - \Delta t/C_n \sum_{j=t_0}^{t} i(j) \end{aligned} \tag{1}$$

$$V(t) = U_{ocv} - V_1 - i(t)R_0, \tag{2}$$

where Δt is the sampling time interval in seconds, C_n is the nominal capacity of the battery, measured in ampere-second As. V_1 is the voltage of the RC sub-circuit, $V(t)$ is the terminal voltage, t_0 is the initial time step. In this study, the charging current $i(t)$ is assigned as negative.

For simplicity, the open-circuit voltage U_{ocv} is modeled as a function of the battery SOC and expressed as f_{ocv}:

$$U_{ocv}(t) = f_{ocv}(soc(t)). \tag{3}$$

The internal resistance R_0 is represented as a function of the internal battery temperature T_{in} of the battery, given by f_R:

$$R_0 = f_R(T_{in}(t)). \tag{4}$$

where f_{ocv} and f_R are implemented using look-up tables, as detailed in the following section.

A first-order RC sub-circuit is employed to represent the slow-varying diffusion voltage within the battery cell, under the assumption that the load current remains constant over each sampling interval. Consequently, the voltage V_1 is obtained based on the dynamic behavior of the corresponding RC network.

$$V_1(t) = a_1 V_1(t-1) + b_1 i(t-1), \tag{5}$$

where,

$$a_1 = e^{-\frac{\Delta t}{R_1 C_1}}, \tag{6}$$

$$b_1 = R_1(1 - e^{-\frac{\Delta t}{R_1 C_1}}), \tag{7}$$

By combining the above equations, the electric sub-model for a Lithium-ion battery can be described as follows:

$$\begin{cases} soc(t) = soc(t-1) - \Delta t/C_n * i(t-1) \\ V_1(t) = a_1 V_1(t-1) + b_1 i(t-1) \\ V(t) = U_{ocv} - i(t) * f_R(T_{in}(t)) - V_1(t) \end{cases} \tag{8}$$

2.2. Battery thermal model

During the operation of a battery, heat is generated within the cell and conducted to the surface before ultimately dissipating into the surrounding environment. Temperature is a critical factor that affects both battery performance and degradation. In general, a battery thermal sub-model consists of three fundamental components: heat generation within the cell, heat conduction through the battery structure, and boundary conditions governing the heat exchange with the ambient environment.

The battery heat generation arises from multiple sources, including the ohmic resistance, electrolyte decomposition, and side reactions. The ohmic component, determined by the direct-current resistance of the electrodes and internal materials, restricts current flow and converts electrical energy into heat. When the battery operates within a safe voltage and temperature range, ohmic heating is typically the dominant source, whereas the contributions from electrolyte decomposition and side reactions are negligible [33]. Therefore, in this study, the heat generation is modeled as follows:

$$Q_J = i(t)^2 R_0 \tag{9}$$

The energy balance equation, derived from the law of energy conservation, forms the basis for computing heat generation and dissipation within the battery. In this study, a simplified lumped thermal sub-model is adopted, which assumes uniform temperature across the internal and surface regions and a spatially uniform heat generation rate. The ambient temperature is treated as constant. Under these assumptions, a lumped thermal model with fixed boundary conditions is formulated based on the energy balance equation:

$$\begin{cases} C_{p1}\frac{dT_{in}}{dt} = Q_J + k_1\left(T_{sf} - T_{in}\right) \\ C_{p2}\frac{dT_{sf}}{dt} = k_1\left(T_{in} - T_{sf}\right) + k_2\left(T_a - T_{sf}\right) \end{cases} \tag{10}$$

where T_{in} denotes the battery internal temperature, T_{sf} is the battery surface temperature. T_a is the ambient temperature. Q_J denotes the ohmic internal resistance heat. C_{p1} and C_{p2} are the heat capacities of the battery interior and the shell, respectively. k_1 is the heat transfer coefficient between the battery and the shell. k_2 is the heat transfer coefficient between the battery shell and the environment. To express the thermal model in discrete time, the following definitions are introduced:

$$\frac{dT(t)}{dt} = \frac{z-1}{\Delta t} * T(t) = \frac{1}{\Delta t} * (T(t+1) - T(t)). \tag{11}$$

Then, the final battery thermal model with internal temperature dynamics in discrete time is formulated as follows:

$$\begin{cases} T_{in}(t+1) = \left(1 - \Delta t\frac{k_1}{C_{p1}}\right)T_{in}(t) + \Delta t\frac{k_1}{C_{p1}}T_{sf}(t) + \\ \qquad \frac{\Delta t}{C_{p1}}(i(t)^2 R_0) \\ T_{sf}(t+1) = \Delta t\frac{k_1}{C_{p2}}T_{in}(t) + \left(1 - \Delta t\frac{k_1+k_2}{C_{p1}}\right)T_{sf}(t) + \\ \qquad k_2 T_a\frac{\Delta t}{C_{p2}} \end{cases} \tag{12}$$

2.3. Complete thermoelectric model

In this study, the battery charging process is formulated as an optimal control problem executed over repetitive iterations. Given the nonlinear coupling between the electrical and thermal states with respect to the input current. To ensure the application of convex optimization in the general MPC framework, a cascading linearized thermoelectric battery model is introduced as follows:

Battery thermal sub-model:

$$x_T(t+1) = A_T * x_T(t) + B_T * u(t) + C_T(t), \tag{13}$$

where $x_T(t) = [T_{in}(t), T_{sf}(t)]^T$ $C_T = [0, k_2 T_a \Delta t/C_{p2}]^T$. $u(t) = i(t)^2$. The other system matrices are defined as follows:

$$A_T = \begin{bmatrix} 1 - \Delta t\frac{k_1}{C_{p1}} & \Delta t\frac{k_1}{C_{p1}} \\ \Delta t\frac{k_1}{C_{p2}} & 1 - \Delta t\frac{k_1+k_2}{C_{p1}} \end{bmatrix}, \quad B_T = \begin{bmatrix} \frac{\Delta t R_0}{C_{p1}} \\ 0 \end{bmatrix} \tag{14}$$

Battery electric sub-model:

$$\begin{cases} x_E(t+1) = A_E * x_E(t) + B_E * u'(t) \\ V(t) = f_{ocv}(soc(t)) - i(t) * f_R(T_{in}(t)) - V_1(t) \end{cases} \tag{15}$$

where $x_E(t) = [soc(t), V_1(t)]^T$, $u'(t) = i(t)$,

$$A_E = \begin{bmatrix} 1 & 0 \\ 0 & a_1 \end{bmatrix}, \quad B_E = \begin{bmatrix} -\Delta t/C_n \\ b_1 \end{bmatrix} \tag{16}$$

In the proposed cascaded linearized thermoelectric model, the nonlinear coupling between the thermal dynamics and the electrical subsystem is captured by the relationship $u(t) = u'(t)^2$, where $u'(t) = i(t)$ denotes the actual charging current. Under this formulation, the two linearized sub-models are hierarchically integrated within the control framework to ensure simultaneous regulation of the internal temperature and electrical states.

3. Historical data-driven self-learning control

The model predictive control (MPC) is widely applied in practical engineering systems, where a predictive model is used to estimate future system behavior and evaluate a cost function over a finite horizon. Based on these predictions, the MPC computes the optimal control inputs to achieve the desired performance. However, the effectiveness of the conventional MPC depends heavily on model accuracy and robustness. To improve control performance, this work proposes a historical data-driven self-learning framework that iteratively refines the control strategy using accumulated operational data. In the proposed approach, historical state-mapped constraints and a memory function, which represent the minimum cumulative future cost inferred from past data, are incorporated into the MPC formulation to iteratively optimize the control input trajectory.

3.1. Self-learning MPC formulation

To continuously improve control performance using historical state data, the battery thermal sub-model is reformulated as a prediction model, where the predicted state $\hat{x}_k(j|t)$ and the predicted control input $u_k(j|t)$ satisfy the following general expression:

$$\hat{x}_k(j+1 \mid t) = A\hat{x}_k(j \mid t) + Bu_k(j \mid t) + C(t+i), \tag{17}$$

where $j = 0, 1, \ldots, N_p - 1$, N_p denotes the prediction horizon. k is the iteration number. The initial predicted state is defined as $\hat{x}_k(0 \mid t) = x_k(t)$. The system matrices are defined as $A \in \mathbb{R}^{n\times n}$, $B \in \mathbb{R}^{n\times m}$, $C \in \mathbb{R}^n$.

The control objective is to monitor and regulate the battery internal temperature within a safe range while ensuring rapid charging from the initial SOC to the desired setpoint. To achieve this objective within the MPC framework, an appropriately designed cost function has been formulated as follows:

$$\begin{aligned} J_k(t) &= \sum_{i=0}^{N_p-1} L_k([\hat{x}_k(j+1 \mid t) - x_r(t+j)], \delta u_k(j \mid t)) \\ &= \sum_{j=0}^{N_p-1} [\hat{x}_k(j+1 \mid t) - x_r(t+j)]^T Q[\hat{x}_k(j+1 \mid t) \\ &\quad - x_r(t+j)] + \delta u_k^T(j \mid t) H \delta u_k(j \mid t), \end{aligned} \tag{18}$$

where Q and H are weighting factors that are adopted to balance the significance of the control performance and the input variation cost. The term x_r denotes the reference state trajectory, $\delta u_k(j \mid t) = u_k(j \mid t) - u_k(j-1 \mid t)$ is the predicted control increment sequence. This formulation ensures a balanced consideration of both the system tracking performance and the efficiency of the control input.

Constraints are inherent in practical engineering systems, with their permissible ranges typically defined by physical limitations and safety regulations. Therefore, it is essential to ensure that the optimal solution obtained under a given cost function satisfies these constraints during control algorithm development. For the system model under consideration, it is assumed that constraints are imposed on both the system states and control inputs, as defined below:

$$u_{min} \le u_k(t) \le u_{max}, \quad x_{min} \le x_k(t) \le x_{max}. \tag{19}$$

The general formulations of the constraints can be rewritten as:

$$\Gamma^u u_k(t) \le \Lambda_k^u(t), \quad \Gamma^x x_k(t) \le \Lambda_k^x(t), \tag{20}$$

where $\Gamma^u \in \mathbb{R}^{2m\times m}$, $\Gamma^x \in \mathbb{R}^{2n\times n}$,

$$\Gamma^u = \begin{bmatrix} I_m \\ -I_m \end{bmatrix}, \quad \Gamma^x = \begin{bmatrix} I_n \\ -I_n \end{bmatrix} \tag{21}$$

Then, a general constrained dynamic optimization problem is formulated as follows:

$$\begin{aligned} \min_{\mathbf{u}_k(t)} & \sum_{j=0}^{N_p-1} [\hat{x}_k(j+1 \mid t) - x_r(t+j)]^T Q[\hat{x}_k(j+1 \mid t) \\ & - x_r(t+j)] + \delta u_k^T(j \mid t) H \delta u_k(j \mid t) \\ & s.t. \\ & \hat{x}_k(j+1 \mid t) = A\hat{x}_k(j \mid t) + Bu_k(j \mid t) + C(t+i), \\ & \Gamma^u u_k(t) \le \Lambda_k^u(t), \quad \Gamma^x x_k(t) \le \Lambda_k^x(t). \end{aligned} \tag{22}$$

3.2. Formulation of historical states and memory function datasets

Solving the optimization problem defined in Eq. (22) based solely on the predictive model and system constraints may lead to unreliable outcomes, particularly in complex or uncertain environments. To enhance the evaluation of the potential contribution of historical state information and input data in optimizing future control input trajectories, a novel memory function is introduced. This function leverages historical system states $x_k(t)$ and input variations $\delta u_k(t)$ to estimate the minimum achievable cumulative cost associated with corresponding state-input pairs. The formulation of the memory function is presented as follows:

$$\begin{aligned} M_k(N) &= L_k(x_k(N+1), \delta u_k(N)) \\ &= x_k(N+1)^T Q x_k(N+1) + \delta u_k(N)^T H \delta u_k(N), \end{aligned} \tag{23}$$

$$M_k(t) = L_k(x_k(t+1), \delta u_k(t)) + M_k(t+1), \quad t < N \tag{24}$$

It is noteworthy that the memory function is evaluated in a backward recursive manner. Specifically, for each iteration, the terminal memory function value $M_k(N)$ is evaluated first. The memory function at each preceding time step is then recursively determined by moving backward in time, utilizing the previously computed memory value and the cost function at the current time step. This backward recursive structure progressively reduces the cumulative estimated future costs as the computation approaches the beginning of the iteration. By leveraging the computed memory function in conjunction with the historical data from the previous iteration $(k-1)$, the sets of historical state information and their associated memory function values can be systematically constructed as follows:

$$\mathbf{X}_{k-1} = \left\{ x_{k-1}(0), x_{k-1}(1), \ldots, x_{k-1}(N) \right\}, \tag{25}$$

$$\mathbf{M}_{k-1} = \left\{ M_{k-1}(0), M_{k-1}(1), \ldots, M_{k-1}(N) \right\}. \tag{26}$$

3.3. Development of convex mapping constraints

To enable the integration of historical trajectories into the current optimization process, a convex hull encompassing all possible convex combinations of historical states is constructed through convex optimization techniques. This convex hull represents a set of points formed by weighted combinations of historical states, subject to the following conditions:

$$y = \sum_{j=1}^{r} \theta_j x_j, \tag{27}$$

$$\sum_{j=1}^{r} \theta_j = 1, \theta_j \ge 0, j = 1, \ldots, r, \tag{28}$$

where θ is the coefficient, r is the number of the elements in x. x can be a vector, scalar, or point in an affine space. The convex hull of a set $\mathbf{C}$, denoted as $\mathbf{convC}$, is defined as the set of all convex combinations of points in $\mathbf{C}$ [34], as follows:

$$\mathbf{convC} = \left\{ \sum_{j=1}^{r} \theta_j x_j \mid x_j \in C, \theta_j \geq 0, j = 1, \ldots, r, \sum_{j=1}^{r} \theta_j = 1 \right\} \tag{29}$$

Building upon the above convex optimization preliminaries, convex hulls of the memory function and historical states, which incorporate information previously interacted with the system in the past iterations, are constructed to refine the last control input in the prediction horizon of the current iteration. The mathematical formulations of the defined convex hulls are presented as follows:

$$\mathbf{conv}M_{k-1}(t) = \left\{ \sum_{j=-d}^{d} \theta_{k-1,j} M_{k-1}(t+j) \right\}, \tag{30}$$

$$\mathbf{conv}X_{k-1}(t) = \left\{ \sum_{j=-d}^{d} \theta_{k-1,j} X_{k-1}(t+j) \right\}, \tag{31}$$

where d is the window size of the historical data to be employed, and

$$\theta_{k-1,j} \geq 0, and \sum_{j=-d}^{d} \theta_{k-1,j} = 1 \tag{32}$$

To integrate the derived convex hulls into the control framework and refine the solution obtained from the general MPC formulation, a convex hull constraint based on the historical state information is imposed on the last predicted state $\hat{x}_k(N_p \mid t)$. This constraint ensures that the last state in the prediction horizon remains within the convex hull of the historical state set $\mathbf{X}_{k-1}$, thereby contributing to the stability of the closed-loop system.

$$\hat{x}_k(N_p \mid t) = \sum_{j=-d}^{d} \theta_{k-1,j} X_{k-1}(t + N_p + j). \tag{33}$$

Then, the cost function is augmented by the corresponding smallest convex hull of the memory function dataset $\mathbf{conv}M_{k-1}(t+N_p)$. The lifted formulation of the new cost function is defined as follows:

$$J_k'(t) = J_k(t) + \sum_{j=-d}^{d} \theta_{k-1,j} M_{k-1}(t + N_p + j), \tag{34}$$

where all the non-negative coefficients $\theta_{k-1,j}$ are the same as those used in the convex hull of historical states in Eq. (33).

Thereby, the optimization problem (22) is reformulated as the minimization of the index with respect to the control input $\mathbf{u}_k(t)$ and coefficients $\theta_{k-1,j}$.

$$\begin{aligned} \min_{\theta_{k-1,j}\mathbf{u}_k(t)} & J_k(t) + \sum_{j=-d}^{d} \theta_{k-1,j} M_{k-1}(t + N_p + j) \\ & s.t. \\ & \hat{x}_k(j+1 \mid t) = A\hat{x}_k(j \mid t) + Bu_k(j \mid t) + C(t+i), \\ & \Gamma^u u_k(t) \leq \Lambda_k^u(t), \quad \Gamma^x x_k(t) \leq \Lambda_k^x(t), \\ & \theta_{k-1,j} \geq 0, and \sum_{j=-d}^{d} \theta_{k-1,j} = 1, \\ & \hat{x}_k(N_p \mid t) = \sum_{j=-d}^{d} \theta_{k-1,j} X_{k-1}(t + N_p + j) \end{aligned} \tag{35}$$

Fig. 2 intuitively illustrates the convex mapping process using the historical state data $x_{k-1}(t)$ and memory function $M_{k-1}(t)$. Specifically, the proposed historical data-driven self-learning control algorithm utilizes the convex mapping constraints derived from the historical states and the smallest memory function convex hull within the d-neighbor $[t-d, t+d]$ at time step t of the previous iteration to optimize the control input in the current iteration.

The core idea of the memory-function–enhanced cost formulation is to evaluate the contribution of the historical dataset and to constrain the terminal predicted state within the resulting convex region using

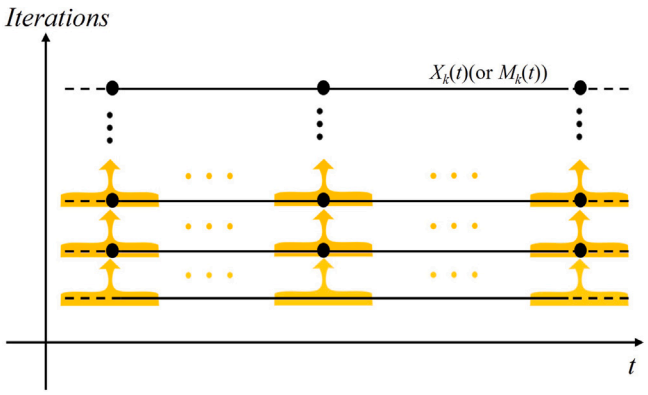

Fig. 2. Historical data convex mapping.

an optimized coefficient. This guarantees that the terminal predicted state always lies within the convex hull of the historical state set, thereby enabling continuous refinement of the control input trajectory. Importantly, the memory function is integrated in a way that preserves the standard quadratic MPC cost structure and maintains the generalizability of the loss function. In addition, the memory-function term is constructed from stored historical data, which is known at each computation step and does not introduce extra uncertainty into the optimization.

Additionally, to enhance the consistency and stability of the proposed algorithm, the historical state data and the corresponding memory function values at the initial and terminal sampling time steps are augmented in accordance with the following expressions:

$$\begin{cases} X_{k-1}(0+j) = X_{k-1}(0), & -d \leq j \leq 0 \\ M_{k-1}(0+j) = M_{k-1}(0), & -d \leq j \leq 0 \\ X_{k-1}(N+d) = X_{k-1}(N), & 0 \leq j \leq d \\ M_{k-1}(N+d) = M_{k-1}(N), & 0 \leq j \leq d \end{cases} \tag{36}$$

At each time step t of the kth iteration, the memory function-enhanced optimization problem defined in Eq. (35) is solved to obtain the optimal control input sequence $\mathbf{u}_k^*(t)$. The first element of this sequence is then applied to the system model, as expressed below:

$$u_k^*(t) = [1, 0, \ldots, 0]\mathbf{u}_k^*(t). \tag{37}$$

The proposed memory function-enhanced control strategy utilizes the historical state information to refine the control input trajectory at each iteration, improving both the accuracy and efficiency over the conventional MPC approach. As illustrated in Fig. 3, the proposed historical data-driven self-learning control framework operates through a closed-loop iterative process. At each iteration, the control input is updated based on the historical state information and the resulting system response, which is subsequently stored and fed back to initialize the next iteration. This iterative feedback mechanism enables continuous refinement of the control policy and ensures stable convergence of the control process.

4. Overall control framework for battery charging process

4.1. Battery model parameters

In this study, the parameters used in the thermo-electric battery model were adopted from our previous works [35,36], in which identical electrical and thermal sub-model structures were employed. In these works, a comprehensive parameter identification was experimentally conducted on a prismatic $LiFePO_4$-Graphite battery, with a nominal capacity of 10 Ah and a nominal voltage of 3.2 V. Furthermore, since embedding micro-sensors within the cell core is experimentally

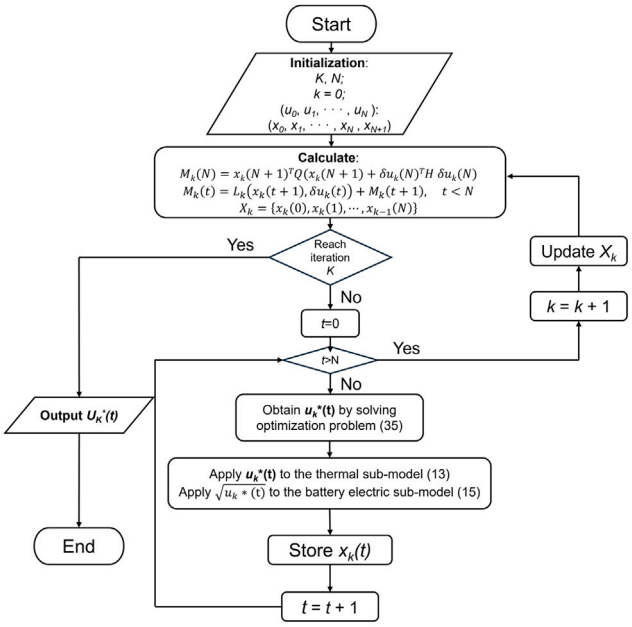

Fig. 3. The flowchart of the proposed historical data-driven self-learning control framework.

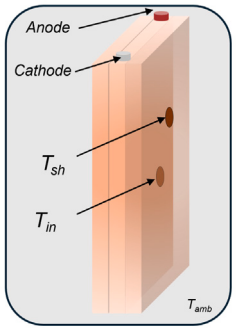

Fig. 4. Battery thermal model.

challenging, internal temperature measurements were approximated using a three-sub-cell configuration, in which both central and surface temperatures were instrumented, as illustrated in Fig. 4. The identified parameters were rigorously validated through a direct comparison between model simulations and experimental measurements for both the electrical and thermal subsystems, achieving a maximum validation voltage error RMSE of approximately $3.4mv$ and internal temperature RMSE of T_{in} 0.82 °C. The complete experimental setup and measurement procedures are documented in detail in [35], and will not be repeated in this paper due to the page limit.

The parameter identification results are summarized in Table 1, and the functions f_{ocv} and f_R are obtained from look-up tables using linear interpolation, with reference to Tables 2 and 3. In the experiments, the ambient temperature was maintained at 27 °C, while both the initial internal and surface temperatures were set to 29 °C.

According to the safe operating limits of $LiFePO_4$ batteries, constraints on the charging current, terminal voltage, and SOC must be imposed throughout the charging process, with the SOC required to increase from 0.1 to 0.9. According to the battery properties of the studied $LiFePO_4$-Graphite battery, the applied current is limited to 30 A at a 3C charging rate. The constraint for voltage V_{max} is set as 3.65 V, which is typically a cut-off voltage for $LiFePO_4$ batteries.

Table 1
Model parameters.

Parameters	Values	Unit
a_1	0.981	–
b_1	1.8e−4	–
k_1	1.264	$Wm^{-1}K^{-1}$
k_2	0.33	$Wm^{-1}K^{-1}$
C_{p1}	263.8	$Jkg^{-1}K^{-1}$
C_{p2}	31.2	$Jkg^{-1}K^{-1}$
C_n	36 000	As

Table 2
SOC and U_{ocv}.

SOC	0.9	0.798	0.695	0.593	0.491	0.389	0.287	0.186	0.085
$U_{ocv}(V)$	3.33	3.325	3.299	3.292	3.290	3.278	3.251	3.215	3.057

Table 3
T_{in} and R_0.

T_{in} (°C)	−10	0	10	23	32	39	52
R_0 (Ω)	0.0259	0.0180	0.0164	0.0152	0.0125	0.0124	0.0120

In the implementation, the maximum charging current rate constraint is applied as a standard input constraint within the MPC formulation. Since the optimization variable is defined as the scaled input $u(t) = i(t)^2$ in thermal sub-model, the original bound $-30\,\text{A} \le i(t) \le 0\,\text{A}$ is equivalently expressed as

$$0 \le u(t) \le 900. \tag{38}$$

The terminal voltage constraint

$$2.6\,\text{V} \le V(t) \le 3.65\,\text{V} \tag{39}$$

is also reformulated into an input-dependent constraint through the electric sub-model. Through the relation

$$V(t) = U_{\text{ocv}}\big(soc(t)\big) - i(t) \cdot f_R\left(T_{\text{in}}(t)\right) - V_1(t), \tag{40}$$

the upper voltage limit $V(t) \le 3.65\,\text{V}$ yields a current-dependent inequality

$$i(t) \ge \frac{U_{\text{ocv}}\big(soc(t)\big) - V_1(t) - 3.65}{f_R\big(T_{\text{in}}(t)\big)}. \tag{41}$$

Since the charging current is defined as negative in this study ($i(t) = -\sqrt{u(t)}$), the above constraint can be converted into an admissible bound on the input $u(t)$ at each sampling step:

$$u(t) \le \left(\frac{U_{\text{ocv}}\big(soc(t)\big) - V_1(t) - 3.65}{f_R\big(T_{\text{in}}(t)\big)}\right)^2. \tag{42}$$

All quantities on the right-hand side are known at the current time step, meaning that the resulting constraint remains linear with respect to the optimization variable and can be enforced directly within the MPC framework while ensuring voltage safety.

The SOC constraint is defined as

$$0.1 \le soc(t) \le 0.9. \tag{43}$$

By reformulating the current and voltage limits into input-compatible expressions, all safety requirements are enforced explicitly within the MPC solver without introducing additional nonlinear state constraints, thereby maintaining both computational tractability and operational safety throughout the charging process.

4.2. Control framework

The primary objective of this study is to address the challenge of regulating the battery internal temperature within a designed safety

Algorithm 1 Historical data-driven self-learning control algorithm for battery charging process.

Given: K: number of iterations;
N: control length in one iteration;
N_p: MPC prediction horizon;
$(u_0, u_1, \cdots, u_N)$:initial action sequence following the CC-CV charging profile;
$(x_0, x_1, \cdots, x_N, x_{N+1})$: initial state sequence following the CC-CV charging profile;
Q, H: weighting factors in the cost function;

for $k = 1$ to K **do**
  $x_k(0) \leftarrow x_0$
  $u_k(0) \leftarrow u_0$
  if $k == 1$ **then**
    Calculate initial memory function set **M** and state set **X** from initial state sequence;
  end if
  for $t = 1$ to N **do**
    Obtain $u_k^*(t)$ by solving optimization problem (35);
    $u_k'^*(t) \leftarrow -\sqrt{u_k^*(t)}$;
    Apply $u_k^*(t)$ to the battery thermal sub-model (13) and $u_k'^*(t)$ to the battery electric sub-model (15) to obtain battery states $x_k(t)$;
  end for
  $M_k(N) = x_k(N+1)^T Q(x_k(N+1) + \delta u_k(N)^T H \delta u_k(N)$;
  $M_k(t) = L_k(x_k(t+1), \delta u_k(t)) + M_k(t+1), \quad t < N$;
  $\mathbf{X}_k = \{x_k(0), x_k(1), \cdots, x_k(N)\}$,
end for

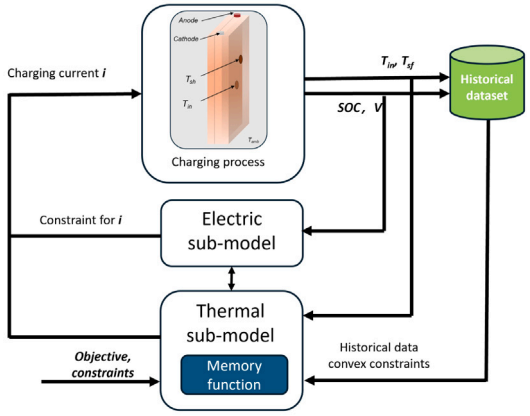

Fig. 5. Control framework.

threshold while achieving a rapid charging process. Algorithm 1 provides the control procedure of the proposed historical data-driven self-learning control approach for the battery charging process. In this control strategy, to ensure the application of convex constraints from both battery electric and thermal models, the primary control logic is applied to the battery thermal sub-model, and the battery electric sub-model is linked through the nonlinear connection of the model inputs to enforce constraints on the electric states.

Fig. 5 intuitively illustrates the overall control framework. In the implementation of the proposed battery charging control framework, the battery thermal sub-model is treated as the primary model within the self-learning MPC framework, while the electric sub-model functions as a subordinate model for monitoring the battery electrical states. Consequently, the thermal sub-model states are directly formulated into the cost function in the MPC framework. In contrast, constraints from the electric sub-model are enforced by converting the state constraints into equivalent constraints on the charging current, thereby regulating the direct control input $u_k(t)$, ensuring safe and efficient charging operation on both thermal and electric states.

5. Results and discussion

5.1. Validation of cascaded model constraints

To evaluate the impact of state constraints from the cascaded sub-model, a comparative study was performed with and without enforcing the terminal-voltage constraint. The controller was configured with: the number of iterations K is set to 10, the prediction horizon is $N_p = 15$, the weighting factors in the cost function $Q = diag[10, 0], H = 20$, and the internal temperature constraint is set to 38 °C. The results are shown in Fig. 6.

When the terminal-voltage constraint is not applied (Fig. 6(a)), the charging-current trajectories become progressively smoother across iterations, demonstrating the self-learning capability of the proposed framework. However, the terminal voltage exceeds the allowable limit (Fig. 6(a2)) because the controller prioritizes rapid charging. In contrast, when the voltage constraint is enforced, the terminal voltage (Fig. 6(b2)) remains consistently below the prescribed upper bound. The internal temperature stays stable once reaching the threshold, as shown in Figs. 6(a3) and 6(b3).

These results confirm both the effectiveness and necessity of incorporating state constraints from the cascaded electrical sub-model, and demonstrate the stable convergence and strong self-learning capability of the proposed historical-data-driven convex-mapping strategy.

5.2. Effect of prediction horizons

The prediction horizon N_p plays a crucial role in balancing control performance and computational burden. Fig. 7 displays the system response under different N_p configurations in a matrix format, where the rows (a)–(c) correspond to N_p values of 15, 30, and 45, respectively, while the columns (1)–(3) represent the optimized control current trajectory, terminal voltage output, and internal temperature evolution profile over 10 iterations.

As shown in Figs. 7 (a1), (b1), and (c1), increasing N_p noticeably reduces the fluctuation of the optimized charging current, leading to improved control stability. At N_p=45, the charging current trajectories exhibit considerable stability even in the early stages of the iteration process, achieving faster convergence compared to N_p=15. Fig. 7 (a2), (b2), and (c2) illustrate the terminal voltage outputs. Due to the constraints imposed by the cascaded electric sub-model, all terminal voltage outputs are consistently maintained below 3.65 V. Additionally, as N_p increases, A similar stabilization effect is observed in the terminal voltage outputs. Figs. 7 (a3), (b3), and (c3) illustrate the evolution of the battery internal temperature. Since the internal temperature is the primary regulated variable, it is noteworthy that the profiles remain relatively consistent as N_p increases. While larger horizons enhance stability and convergence, they also increase computational cost. Therefore, it is essential to determine an appropriate balance between control performance and computational efficiency according to different application requirements.

5.3. Analysis of weighting factors

In this study, the cost function is formulated to balance control performance in regulating the battery internal temperature and optimizing charging efficiency. The control input and output are significantly influenced by varying weighting factor configurations. Therefore, a comparative analysis is conducted using three distinct configurations: $H = 10$; $H = 20$; $H = 40$, while keeping all other parameters the same, the prediction horizon $N_p = 15$. To explicitly evaluate the impact of the cost function weighting factor, the internal temperature threshold

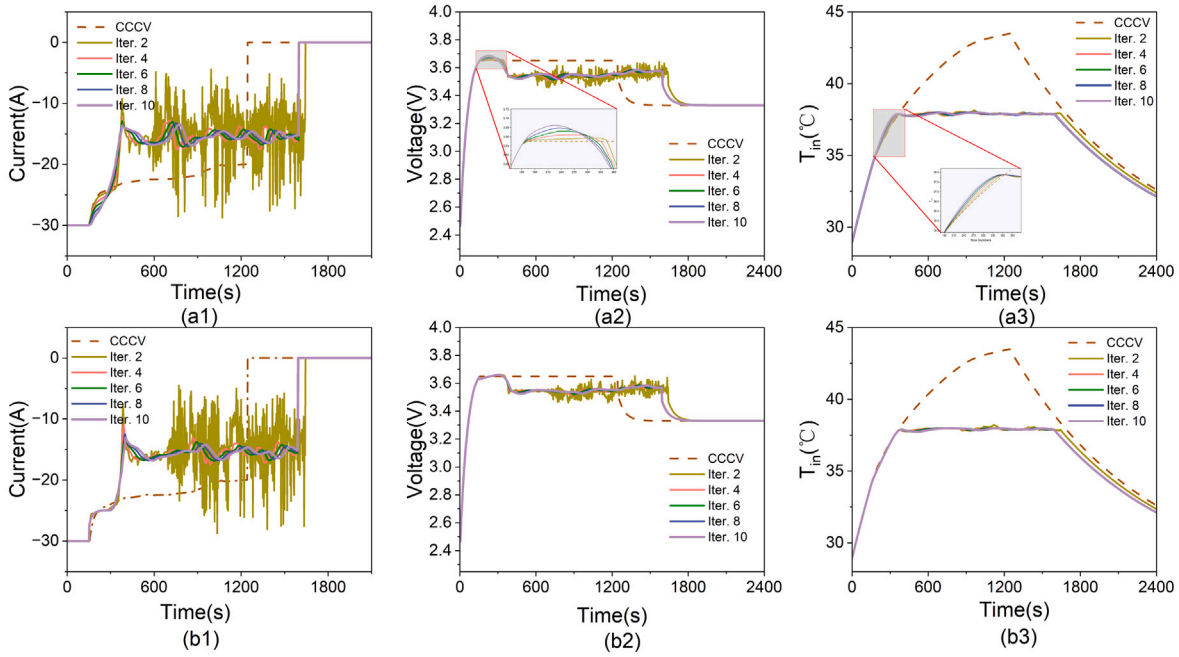

Fig. 6. (a) Results with cascading terminal voltage constraint; (b) Results without cascading terminal voltage constraint. ($N_p = 15, H = 10, T_{in} = 38$ °C).

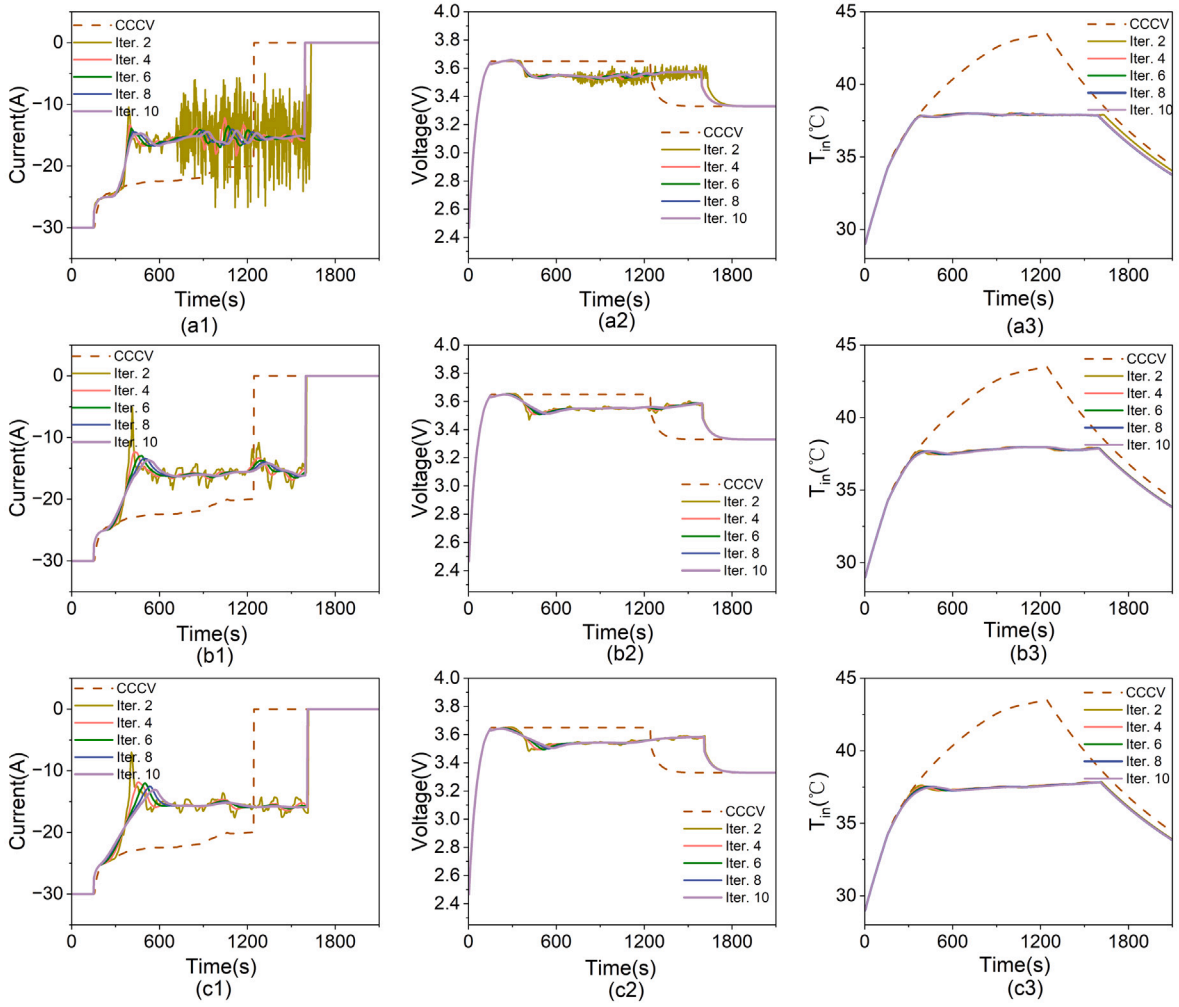

Fig. 7. Effect of different prediction horizons. (a) N_p=15; (b) N_p=30; (c) N_p=45. ($H = 10, T_{in} = 38$ °C).

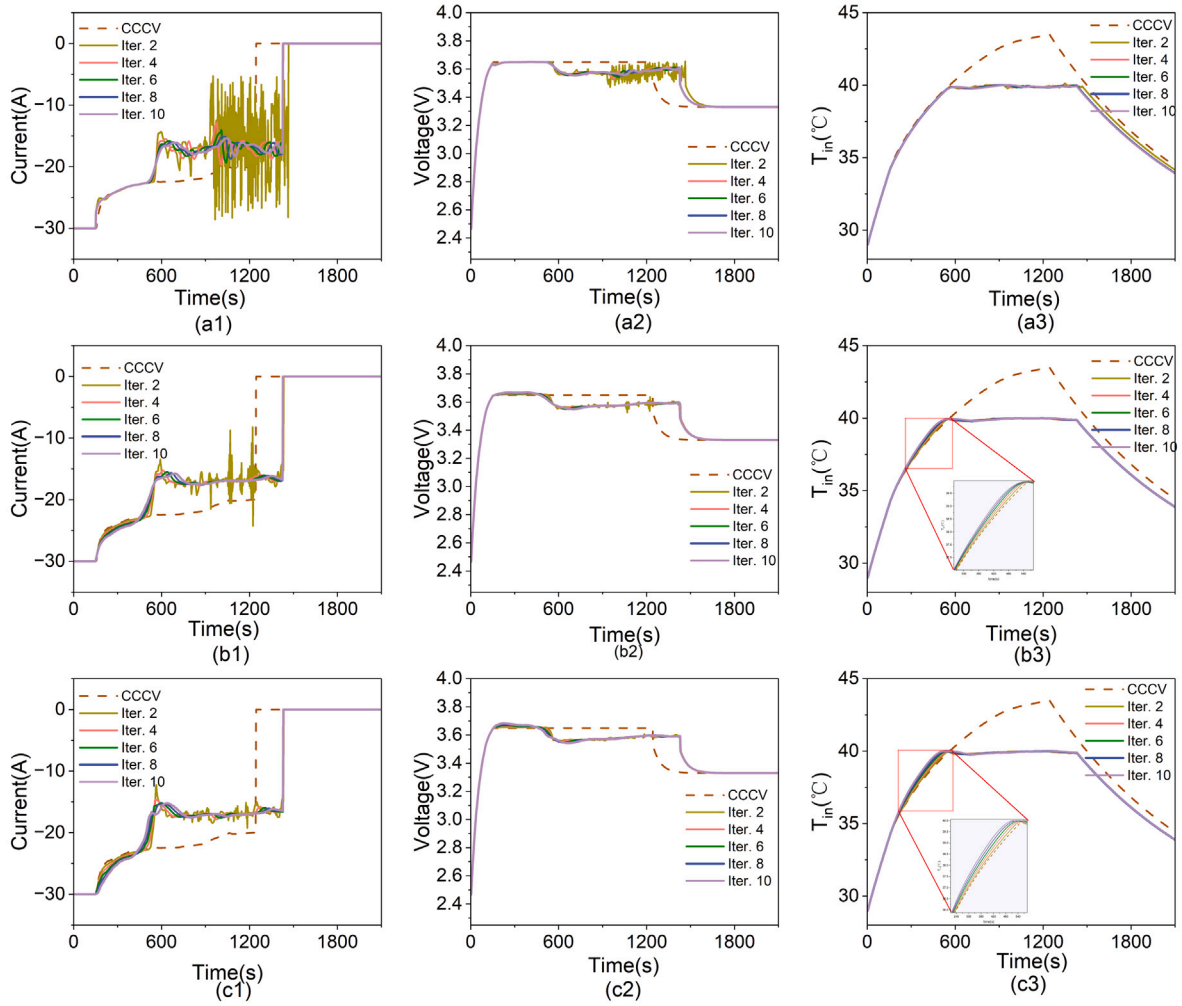

Fig. 8. Effect of various weighting factors. (a) $H = 10$; b) $H = 20$; c) $H = 40$. ($N_p = 15, T_{in} = 40$ °C).

in this simulation is set to 40 °C. Fig. 8 (a), (b), and (c) present the control results for $H = 10$, 20, and 40, respectively. It is evident that as the weighting factor H for the input increment cost increases, the algorithm increasingly prioritizes charging efficiency during the optimization of the charging current trajectory. Specifically, Fig. 8 a(1), a(2), and a(3) demonstrate that a larger H leads to a more stable optimized charging current trajectory. This is primarily due to the increased penalty on δu in the cost function, which effectively suppresses the fluctuation of the control input. in Fig. 8 (b3) and (c3), as the iteration increases, a noticeable rise in battery internal temperature is observed as it approaches the temperature threshold. Furthermore, Fig. 8 (b2) and (c2) exhibit a slight increase in the terminal voltage. These results demonstrate the adaptability of the proposed historical data-driven self-learning control algorithm in balancing various control objectives.

5.4. Robustness analysis under parameter uncertainty

To evaluate the robustness of the proposed method against battery parameter uncertainties, two levels of stochastic perturbations: 5% and 10% Beta distributions were applied to the battery internal resistance and capacity parameters to account for aging and inter-cell variability, defined as:

$$C' \sim C_n \cdot (1 - Beta(2,5) \cdot k_\beta) \tag{44}$$

$$R_0' \sim R_0 \cdot (1 + Beta(2,5) \cdot k_\beta) \tag{45}$$

where $k_\beta \in \{5\%, 10\%\}$ denotes the uncertainty level. The Beta distribution, characterized by finite mean and variance, naturally aligns with the physical constraints of battery parameters, such as bounded internal resistance and capacity variations within finite ranges [27].

The CCCV charging profile is adopted as the initial solution for iterative optimization. Comparative results under both uncertainty levels demonstrate the strong capability of the proposed method. As shown in Figs. 9 (a3) and (b3), the internal temperature remains strictly below the specified threshold 37 °C, demonstrating consistent thermal management performance. The voltage responses (Figs. 9 (a2) and (b2)) confirm that the algorithm effectively maintains the terminal voltage within the safe upper bound of 3.65 V throughout the charging process. Figs. 9 (a1) and (b1) illustrate the evolution of charging current across iterations. Notably, the current profiles under 10% noise exhibit more pronounced fluctuations during the early iterations compared to the 5% case. However, both scenarios ultimately converge to stable and smooth current trajectories in subsequent refinements. The consistency of results between the 5% and 10% noise scenarios demonstrates the inherent robustness of the proposed method to significant parameter uncertainties. These results verify the model fidelity and inherent robustness of the proposed approach with parameter variability and degradation.

5.5. Sensitivity of initial solutions

To investigate the sensitivity of the proposed method to different initial solutions, a comparative study was conducted under a stringent

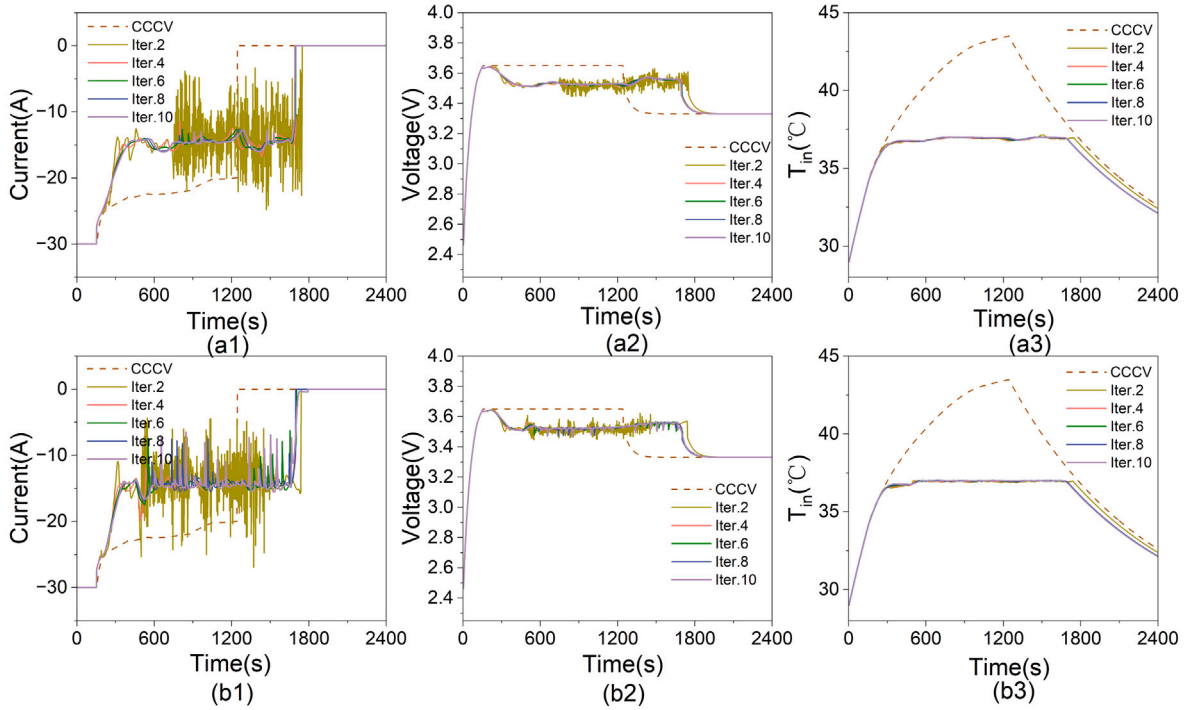

Fig. 9. (a) Results under the 5% *Beta* uncertainty configuration;(b) Results under the 10% *Beta* uncertainty configuration.

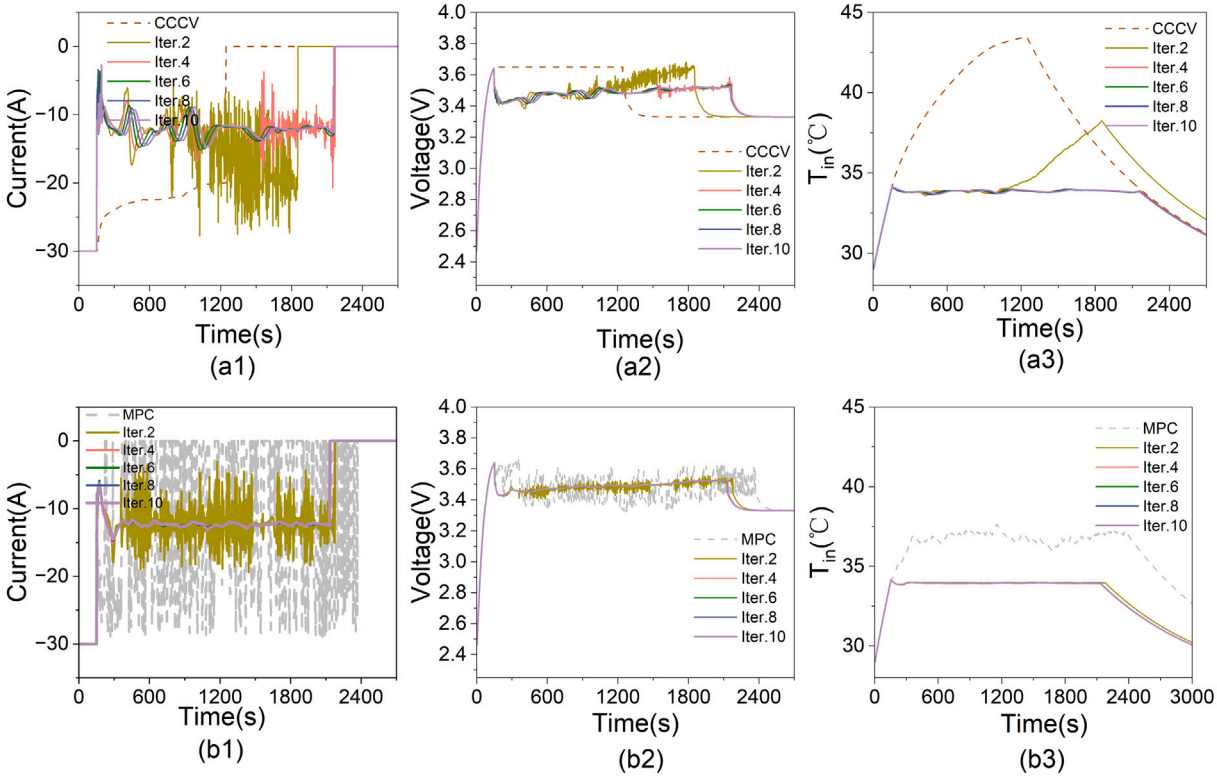

Fig. 10. (a) Results with CCCV initialization;(b) Results with pure MPC initialization.

thermal constraint of 34 °C, representing only a 5 °C margin above the initial battery temperature of 29 °C. Two distinct charging profiles were adopted as the initial references: the conventional CCCV charging profile (Figs. 10 (a1–a3)) and a pure MPC-solved profile (Figs. 10 (b1–b3)). This comparison assesses how the choice of initial solution influences the convergence behavior and control performance of the self-learning control framework under challenging thermal limits.

The results reveal notable differences between the two initialization strategies. When initialized with the CCCV profile, the method experiences mild convergence difficulties during early iterations, as

Table 4
Computation time statistics for different planning horizons.

Horizon	MPC				Ours			
length	Mean	Std	Max	Min	Mean	Std	Max	Min
5	0.094	0.015	0.140	0.081	0.086	**0.004** (↓**73%**)	0.096	0.081
10	0.110	0.017	0.158	0.097	0.105	**0.003** (↓**82%**)	0.120	0.099
20	0.143	0.019	0.202	0.129	0.138	**0.004** (↓**79%**)	0.156	0.131
40	0.199	0.025	0.291	0.179	0.193	**0.005** (↓**80%**)	0.221	0.184

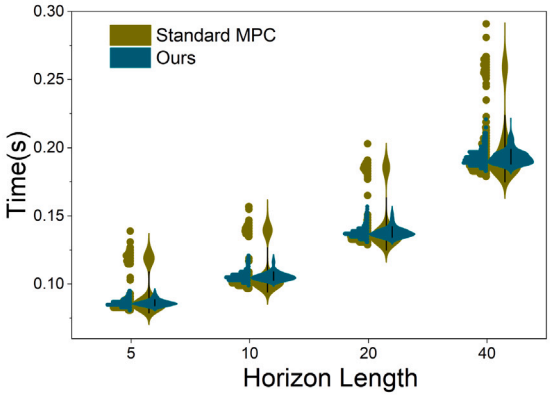

Fig. 11. Computation time comparison.

reflected by fluctuations in the charging current (Fig. 10 (a1)) and insufficient temperature regulation (Fig. 10 (a3)). Nevertheless, the algorithm gradually stabilizes and achieves effective temperature control in subsequent iterations. In contrast, although the initial MPC-based profile itself does not fully satisfy the thermal constraint and produce a stable input trajectory under such a restrictive temperature limit, the proposed method quickly converges toward a smooth and stable charging trajectory. The internal temperature was successfully limited at the specified threshold, and the fluctuations in current profiles were substantially reduced. Additionally, the voltage response (Fig. 10 b2) remains well-regulated within the safety limit of 3.65 V throughout the charging process.

This comparative analysis confirms that initialization strategy plays a critical role in determining the performance of iterative optimization, especially when the feasible region is severely restricted by stringent thermal limits. This sensitivity arises because the proposed convex-mapping constraint is constructed from historical operational data, and the subsequent optimization is guided by the initial reference trajectory. Consequently, an initial solution that provides a more balanced trade-off between charging intensity and thermal safety is preferable, as it facilitates more robust convergence and ensures effective satisfaction of the imposed constraints.

5.6. Computation efficiency analysis

The computation efficiency of the proposed control framework was evaluated across multiple prediction horizon lengths and benchmarked against a standard MPC approach. Table 4 provides detailed statistics of the computation time required to determine the optimal action per step in one iteration. Across all horizon settings, the proposed method achieves mean computation times that are comparable to or slightly lower than those of standard MPC. Notably, the standard deviation of computation time is reduced by approximately 80% compared to the standard MPC, indicating a significantly more stable and predictable computational burden. This improvement can be attributed to the incorporation of the convex mapping constraint, which effectively narrows and refines the feasible solution space, thereby ensuring more stable and consistent solving time costs, even at the longest horizon of 40 steps.

Table 5
Computation time standard deviation comparison (N_p = 10).

Methods	SMPC [27]	DASC [27]	Ours
Std	1.346	**0.003**	**0.003**

Table 5 compares the computation-time standard deviations of the proposed methods with two benchmark charging strategies, namely the Stochastic MPC (SMPC) charging strategy and the learning-driven DAgger-Based Stochastic Control (DASC) method [27]. Notably, the proposed method achieves a computation-time standard deviation of approximately 0.003 with a prediction horizon of 10, which is comparable to that of DASC but significantly lower than that of SMPC. These results confirm the computational stability of the proposed approach and its suitability for real-time battery charging applications, where maintaining predictable and consistent online computation time is essential.

To provide a more intuitive comparison, Fig. 11 visualizes the full distribution of computation times using violin plots. The proposed method exhibits tighter and more concentrated distributions across all horizon lengths, confirming the stable computational behavior. In contrast, standard MPC exhibits heavier upper tails, particularly at longer horizons, indicating a greater chance of occasional prolonged computations. The consistent compact shape of the computation time distributions of the proposed strategy demonstrates improved computation determinism, an essential property for reliable real-time implementation.

These findings confirm the real-time feasibility of the proposed method. The combination of low mean computation time and reduced variability demonstrates that the proposed self-learning MPC framework can effectively optimize control inputs without incurring additional computational burden relative to conventional MPC.

5.7. Evaluation of continuous optimization performance

To evaluate the continuous optimization capability of the proposed data-driven self-learning battery charging control algorithm, Table 6 summarizes the evolution of the mean and standard deviation of the charging current across 10 iterations under different internal temperature limitations. Additionally, to further verify the robustness of the iterative refinement process, the optimization results obtained using both CCCV and standard MPC charging profiles as initial conditions were compared under the stringent temperature limit of 34 °C.

As shown in Table 6, the mean charging current exhibits stable convergence trends across all temperature thresholds. The values gradually increase during the initial iterations to reduce the overall charging duration and then stabilize once convergence is achieved. The reduction in mean current when decreasing the temperature limit further demonstrates the controller's ability to adaptively regulate the charging rate in response to stricter thermal constraints. Moreover, comparisons between the two initialization strategies at 34 °C further indicate that the proposed method effectively mitigates the influence of the initial solution; regardless of whether the process starts from a CCCV-based profile or a standard MPC-generated profile, the mean charging current converges toward nearly identical steady-state values.

Furthermore, the evolution of the standard deviation provides additional information on the smoothness and stability of the optimized trajectories. For all temperature limits, the standard deviation decreases consistently with iterations, confirming that the controller progressively suppresses fluctuations in the charging current. Notably, in the 34 °C$^{(b)}$ case, the initial current exhibits noticeable fluctuation due to the stringent thermal constraint. However, after several iterations, the variability is reduced to comparable variability (about 4.61–4.62). These results collectively confirm the robustness and repeatability of the continuous optimization mechanism, irrespective of the starting solution.

Table 6
Comparisons of Mean and Standard deviation of charging current under different internal temperature limitations.

Iters.	Mean of charging currents						Standard deviation of charging currents					
	40 °C	39 °C	38 °C	37 °C	34 °C$^{(a)}$	34 °C$^{(b)}$	40 °C	39 °C	38 °C	37 °C	34 °C$^{(a)}$	34 °C$^{(b)}$
1	−18.321	−18.097	−16.525	−15.149	−18.186	−13.397	8.350	7.224	7.618	11.120	7.538	**5.194**
2	−19.686	−18.996	−18.000	−15.795	−15.576	−13.242	6.062	5.435	5.118	9.773	6.379	**5.347**
3	−20.189	−19.212	−18.049	−16.682	−13.890	−13.550	4.734	4.836	4.993	5.822	5.433	**4.614**
4	−20.194	−19.219	−18.063	−17.026	−13.301	−13.546	4.693	4.829	4.944	4.948	4.882	**4.610**
5	−20.200	−19.220	−18.069	−17.045	−13.355	−13.537	4.662	4.831	4.917	4.876	4.764	**4.612**
6	−20.213	−19.220	−18.070	−17.057	−13.353	−13.351	4.645	4.833	4.897	4.859	4.752	**4.612**
7	−20.219	−19.220	−18.071	−17.065	−13.346	−13.525	4.629	4.836	4.880	4.847	4.751	**4.612**
8	−20.224	−19.219	−18.069	−17.072	−13.348	−13.517	4.616	4.839	4.866	4.842	4.733	**4.610**
9	−20.225	−19.218	−18.065	−17.086	−13.346	−13.510	4.605	4.841	4.854	4.841	4.730	**4.612**
10	−20.220	−19.217	−18.061	−17.093	−13.354	−13.503	4.601	4.843	4.843	4.839	4.708	**4.614**

34 °C$^{(a)}$ is the result obtained with CCCV charging profile as the initial solution.
34 °C$^{(b)}$ is the result obtained with the standard MPC charging profile as the initial solution.

Table 7
Charging duration improvement compared with a reference charging strategy.

	40 °C	39 °C	38 °C	37 °C	34 °C
GPC [36] (s)	1498	1579	1674	1786	–
Ours (s)	1428	1500	1590	1686	2133
Improvement (s)	70	79	84	100	–

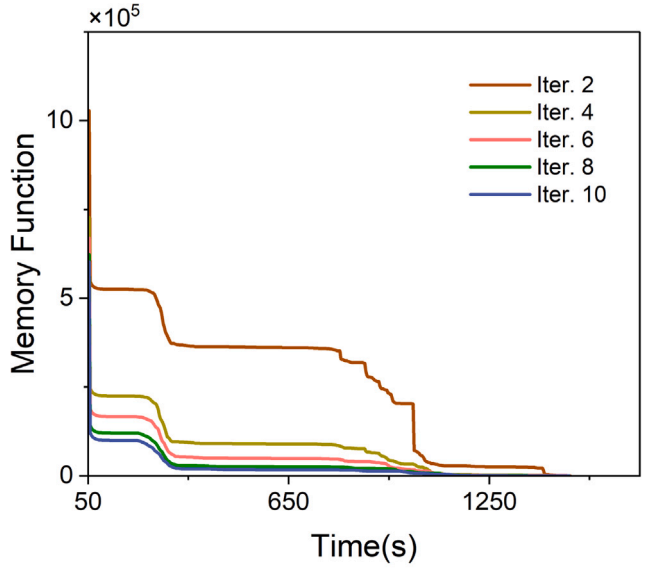

Fig. 12. Memory function evolution. ($N_p = 20, T_{in} = 40$ °C).

Fig. 12 illustrates the evolution of the memory function across iterations. The magnitude of the memory function decreases consistently with the iterations, reflecting the progressive refinement of the internal representation of historical information. This reduction indicates that the proposed historical data-driven self-learning control framework continually improves the control performance and corrective capability, ultimately driving the control process toward stable convergence and effective achievement of charging objectives.

Table 7 compares the charging durations achieved by the proposed control strategy and that of an existing constrained general predictive control (GPC) method [36] under different internal temperature thresholds. Across all comparable temperature limits, the proposed strategy consistently achieves shorter charging durations while satisfying the same thermal constraints. For instance, at 37 °C, the charging duration is reduced by 100 s, with similar improvements observed at other specified temperature thresholds. These results highlight the enhanced charging efficiency delivered by the proposed method and confirm its adaptability in optimizing the charging duration across a range of thermal limitations.

These quantitative results confirm the continuous optimization capability of the proposed method. It iteratively refines both the control accuracy and smoothness of the charging current trajectory, exhibits robustness to different initial conditions, and effectively adapts to stringent temperature constraints. These findings indicate the strong iterative refinement behavior and reliable learning ability of the proposed data-driven self-learning battery charging control algorithm.

6. Conclusions

The battery thermal management is a critical function of the battery management system, particularly under fast charging conditions where thermal impacts on the battery health must be carefully balanced. This study formulates the battery charging process as a repetitive control problem and develops a historical data-driven self-learning control strategy integrated into a model predictive control framework. The main conclusions can be drawn as follows:

(1) A cascading linearized thermoelectric battery model is developed to capture the coupled electrical and thermal dynamics of the battery, including both internal and surface temperature dynamics. This model provides reliable thermal references for control and enables comprehensive performance evaluation.

(2) A novel memory function is incorporated to leverage historical data and apply convex constraints within the self-learning MPC structure. This approach significantly improves the robustness of the proposed method against model uncertainty and parameter variability.

(3) The proposed control strategy effectively maintains the internal battery temperature within safe limits throughout the charging process. In addition, charging efficiency and current trajectory stability are significantly enhanced through the iterative self-learning mechanism.

(4) The convex mapping constraint further improves computational reliability by narrowing and refining the feasible solution space, resulting in more stable and consistent computation times compared to the conventional MPC.

(5) Extensive simulation studies have shown that the proposed control strategy can effectively regulate the internal temperature within a safe range while continuously optimizing the charging efficiency. Furthermore, the computation time variability is significantly reduced, with the standard deviation being decreased by approximately 80% compared to the conventional MPC.

Future work will focus on the experimental validation and practical implementation of the proposed control strategy in real-world battery management systems under various charging conditions, including real-time and online deployment in embedded platforms. In addition, incorporating battery aging models into the control framework will be explored to balance fast charging with long-term degradation, enabling lifetime-aware charging optimization strategies.

CRediT authorship contribution statement

Xiaofei Han: Writing – review & editing, Writing – original draft, Validation, Methodology, Data curation. **Kang Li:** Writing – review & editing, Supervision, Investigation, Conceptualization. **Furong Gao:** Writing – review & editing, Supervision, Methodology, Investigation, Conceptualization. **Yuanqiang Zhou:** Writing – review & editing, Supervision, Methodology, Conceptualization.

Declaration of competing interest

The authors declare that they have no known competing financial interests or personal relationships that could have appeared to influence the work reported in this paper.

Acknowledgments

Xiaofei Han wishes to thank the Chinese Scholarship Council for supporting his research. This work is partially supported by the EPSRC, United Kingdom-funded project 'Networked Energy Hubs for Accelerating Decarbonization of Transport and Energy Sector (UKRI1779)'

Data availability

Data will be made available on request.

References

[1] K.T. Selvi, K.A. Mangai, J.A. Lett, I. Fatimah, S. Sagadevan, Exploring the electrode materials for high-performance lithium-ion batteries for energy storage application, J. Energy Storage 92 (2024) 112208, http://dx.doi.org/10.1016/j.est.2024.112208.

[2] M. Shahjalal, P.K. Roy, T. Shams, A. Fly, J.I. Chowdhury, M.R. Ahmed, K. Liu, A review on second-life of li-ion batteries: prospects, challenges, and issues, Energy 241 (2022) 122881, http://dx.doi.org/10.1016/j.energy.2021.122881.

[3] Y. Wang, W. Li, R. Fang, H. Zhu, Q. Peng, Capacities prediction and correlation analysis for lithium-ion battery-based energy storage system, Control Eng. Pract. 125 (2022) 105224, http://dx.doi.org/10.1016/j.conengprac.2022.105224.

[4] K.M. Tan, T.S. Babu, V.K. Ramachandaramurthy, P. Kasinathan, S.G. Solanki, S.K. Raveendran, Empowering smart grid: A comprehensive review of energy storage technology and application with renewable energy integration, J. Energy Storage 39 (2021) 102591, http://dx.doi.org/10.1016/j.est.2021.102591.

[5] A. Eftekhari, Lithium batteries for electric vehicles: From economy to research strategy, ACS Sustain. Chem. Eng. 7 (6) (2019) 5602–5613, http://dx.doi.org/10.1021/acssuschemeng.8b01494.

[6] K. Liu, Y. Gao, C. Zhu, K. Li, M. Fei, C. Peng, X. Zhang, Q.-L. Han, Electrochemical modeling and parameterization towards control-oriented management of lithium-ion batteries, Control Eng. Pract. 124 (2022) 105176, http://dx.doi.org/10.1016/j.conengprac.2022.105176.

[7] J. Jaguemont, J. Van Mierlo, A comprehensive review of future thermal management systems for battery-electrified vehicles, J. Energy Storage 31 (2020) 101551, http://dx.doi.org/10.1016/j.est.2020.101551.

[8] L. Saw, A.A.O. Tay, L.W. Zhang, Thermal management of lithium-ion battery pack with liquid cooling, in: 2015 31st Thermal Measurement, Modeling & Management Symposium (SEMI-THERM), 2015, pp. 298–302, http://dx.doi.org/10.1109/SEMI-THERM.2015.7100176.

[9] A.A. Pesaran, Battery thermal models for hybrid vehicle simulations, J. Power Sources 110 (2) (2002) 377–382, http://dx.doi.org/10.1016/S0378-7753(02)00200-8.

[10] M. Xu, R. Wang, P. Zhao, X. Wang, Fast charging optimization for lithium-ion batteries based on dynamic programming algorithm and electrochemical-thermal-capacity fade coupled model, J. Power Sources 438 (2019) 227015, http://dx.doi.org/10.1016/j.jpowsour.2019.227015.

[11] J. Liang, Y. Gan, W. Song, M. Tan, Y. Li, Thermal–electrochemical simulation of electrochemical characteristics and temperature difference for a battery module under two-stage fast charging, J. Energy Storage 29 (2020) 101307, http://dx.doi.org/10.1016/j.est.2020.101307.

[12] J. Lin, X. Liu, S. Li, C. Zhang, S. Yang, A.review.on.recent. progress, Challenges and perspective of battery thermal management system, Int. J. Heat Mass Transfer 167 (2021) 120834, http://dx.doi.org/10.1016/j.ijheatmasstransfer.2020.120834.

[13] S. Zhu, C. He, N. Zhao, J. Sha, Data-driven analysis on thermal effects and temperature changes of lithium-ion battery, J. Power Sources 482 (2021) 228983, http://dx.doi.org/10.1016/j.jpowsour.2020.228983.

[14] Y. Wang, X. Chen, C. Li, Y. Yu, G. Zhou, C. Wang, W. Zhao, Temperature prediction of lithium-ion battery based on artificial neural network model, Appl. Therm. Eng. 228 (2023) 120482, http://dx.doi.org/10.1016/j.applthermaleng.2023.120482.

[15] G. Zhang, L. Cao, S. Ge, C.-Y. Wang, C.E. Shaffer, C.D. Rahn, In situ measurement of radial temperature distributions in cylindrical li-ion cells, J. Electrochem. Soc. 161 (10) (2014) A1499, http://dx.doi.org/10.1149/2.0051410jes.

[16] C. Zou, C. Manzie, D. Nešić, Model predictive control for lithium-ion battery optimal charging, IEEE/ASME Trans. Mechatronics 23 (2) (2018) 947–957, http://dx.doi.org/10.1109/TMECH.2018.2798930.

[17] N. Tian, H. Fang, Y. Wang, Real-time optimal lithium-ion battery charging based on explicit model predictive control, IEEE Trans. Ind. Inform. 17 (2) (2021) 1318–1330, http://dx.doi.org/10.1109/TII.2020.2983176.

[18] G.-C. Hsieh, L.-R. Chen, K.-S. Huang, Fuzzy-controlled li-ion battery charge system with active state-of-charge controller, IEEE Trans. Ind. Electron. 48 (3) (2001) 585–593, http://dx.doi.org/10.1109/41.925585.

[19] N. Rahim, S. Mekhilef, E. Chan, H. Ping, Fuzzy-controlled battery charger state-of-charge controller, Int. J. Modelling Simul. 26 (2) (2006) 106–111, http://dx.doi.org/10.1080/02286203.2006.11442357.

[20] D.N.T. How, M.A. Hannan, M.S. Hossain Lipu, P.J. Ker, State of charge estimation for lithium-ion batteries using model-based and data-driven methods: A review, IEEE Access 7 (2019) 136116–136136, http://dx.doi.org/10.1109/ACCESS.2019.2942213.

[21] M.-F. Ng, J. Zhao, Q. Yan, G.J. Conduit, Z.W. Seh, Predicting the state of charge and health of batteries using data-driven machine learning, Nat. Mach. Intell. 2 (3) (2020) 161–170, http://dx.doi.org/10.1038/s42256-020-0156-7.

[22] S. Li, H. He, C. Su, P. Zhao, Data driven battery modeling and management method with aging phenomenon considered, Appl. Energy 275 (2020) 115340, http://dx.doi.org/10.1016/j.apenergy.2020.115340.

[23] Q. Lin, J. Wang, R. Xiong, W. Shen, H. He, Towards a smarter battery management system: A critical review on optimal charging methods of lithium ion batteries, Energy 183 (2019) 220–234, http://dx.doi.org/10.1016/j.energy.2019.06.128.

[24] J.G. Rueda-Escobedo, E. Fridman, J. Schiffer, Data-driven control for linear discrete-time delay systems, IEEE Trans. Autom. Control 67 (7) (2022) 3321–3336, http://dx.doi.org/10.1109/TAC.2021.3096896.

[25] D. Soudbakhsh, A.M. Annaswamy, Y. Wang, S.L. Brunton, J. Gaudio, H. Hussain, D. Vrabie, J. Drgona, D. Filev, Data-driven control: Theory and applications, in: 2023 American Control Conference, ACC, 2023, pp. 1922–1939, http://dx.doi.org/10.23919/ACC55779.2023.10156081.

[26] C. De Persis, P. Tesi, Formulas for data-driven control: Stabilization, optimality, and robustness, IEEE Trans. Autom. Control 65 (3) (2020) 909–924, http://dx.doi.org/10.1109/TAC.2019.2959924.

[27] A. Pozzi, A. Incremona, D. Toti, Imitation learning-driven approximation of stochastic control models, Appl. Intell. 55 (12) (2025) 1–19, http://dx.doi.org/10.1007/s10489-025-06704-x.

[28] J. Drgoňa, J. Arroyo, I. Cupeiro Figueroa, D. Blum, K. Arendt, D. Kim, E.P. Ollé, J. Oravec, M. Wetter, D.L. Vrabie, L. Helsen, All you need to know about model predictive control for buildings, Annu. Rev. Control. 50 (2020) 190–232, http://dx.doi.org/10.1016/j.arcontrol.2020.09.001.

[29] P. Karamanakos, E. Liegmann, T. Geyer, R. Kennel, Model predictive control of power electronic systems: Methods, results, and challenges, IEEE Open J. Ind. Appl. 1 (2020) 95–114, http://dx.doi.org/10.1109/OJIA.2020.3020184.

[30] Y. Zhou, K. Gao, D. Li, Z. Xu, F. Gao, Data-efficient constrained learning for optimal tracking of batch processes, Ind. Eng. Chem. Res. 60 (43) (2021) 15658–15668, http://dx.doi.org/10.1021/acs.iecr.1c0270610.1021/acs.iecr.1c02706.

[31] F. Guo, L.D. Couto, G. Mulder, K. Trad, G. Hu, O. Capron, K. Haghverdi, A systematic review of electrochemical model-based lithium-ion battery state estimation in battery management systems, J. Energy Storage 101 (2024) 113850, http://dx.doi.org/10.1016/j.est.2024.113850.

[32] K. Liu, K. Li, Q. Peng, C. Zhang, A brief review on key technologies in the battery management system of electric vehicles, Front. Mech. Eng. 14 (2019) 47–64, http://dx.doi.org/10.1007/s11465-018-0516-8.

[33] D. Bernardi, E. Pawlikowski, J. Newman, A general energy balance for battery systems, J. Electrochem. Soc. 132 (1) (1985) 5, http://dx.doi.org/10.1149/1.2113792.

[34] S.P. Boyd, L. Vandenberghe, Convex Optimization, Cambridge University Press, 2004.

[35] C. Zhang, K. Li, J. Deng, Real-time estimation of battery internal temperature based on a simplified thermoelectric model, J. Power Sources 302 (2016) 146–154, http://dx.doi.org/10.1016/j.jpowsour.2015.10.052.

[36] K. Liu, K. Li, C. Zhang, Constrained generalized predictive control of battery charging process based on a coupled thermoelectric model, J. Power Sources 347 (2017) 145–158, http://dx.doi.org/10.1016/j.jpowsour.2017.02.039.